Contents lists available at ScienceDirect

Remote Sensing of Environment

Landsat-based detection of mast events in white spruce (*Picea glauca*) forests

Matthew Garcia [a,*], Benjamin Zuckerberg [a], Jalene M. LaMontagne [b], Philip A. Townsend [a]

[a] *Department of Forest and Wildlife Ecology, University of Wisconsin–Madison, 1630 Linden Drive, Madison, WI 53706, USA*
[b] *Department of Biological Sciences, DePaul University, 2325 North Clifton Avenue, Chicago, IL 60614, USA*

ARTICLE INFO

ABSTRACT

Mast seeding in conifers is characterized by the spatially synchronous and temporally variable production of seed cone crops. Large mast seeding events (known as "mast years") can be a visually stunning and ecologically important phenomenon, supporting trophic interactions and survival of seed predators as well as forest regeneration. Documenting patterns in mast seeding is generally labor-intensive, requiring repeated visual cone counts at consistent and widespread locations over long periods to quantify the spatiotemporal variability of cone production. Our goal in this work was to evaluate the correspondence of multispectral vegetation indexes (VIs) from Landsat with ground-based observations of mast seeding in white spruce (*Picea glauca*) forests of the Kluane region, Yukon, Canada. Given the visual characteristics of mast seeding in white spruce, we tested: 1) whether photosynthesis- and color-oriented VIs can identify senescence of spruce cones in late summer and autumn during mast years, and 2) if moisture-oriented VIs can distinguish the significant drying of seed cones from the surrounding spruce canopy vegetation during that senescence and after seeds are released. We hypothesized that the slope of late season decline in VIs in spruce forests would be related to masting (*i.e.*, greater decline in VI during mast years). Using generalized linear mixed-effects modeling (GLMM), we compared more than 100 site-year combinations of mast/non-mast observations to develop VI-based regressions. We found some success identifying mast years with moisture-oriented VIs, while models using the photosynthesis- and color-oriented VIs were not supported, given the data. However, we found that models containing multiple VIs from both categories were more successful than any single-VI model, accurately predicting four of sixteen mast events in site observations. We provide compelling evidence that mast-seeding patterns may be detectable using moisture-oriented Landsat observations over large coniferous forest areas. Additional work is warranted to distinguish the signal for mast events from confounding disturbance-related effects and to differentiate variation in VI signals attributable to masting productivity in contrast to effects of climatological variability on reflectance.

1. Introduction

Mast seeding is the spatially synchronous, temporally variable production of seed crops by populations of perennial plants (Kelly, 1994) and occurs over a range of spatial scales, from hundreds of meters to thousands of kilometers (Koenig and Knops, 1998; LaMontagne et al., 2020). "Mast years" are those in which very large seed crops are produced (LaMontagne and Boutin, 2009) and are a visually stunning and ecologically significant event: an evergreen coniferous forest canopy can turn brown in late summer and autumn with opened and drying seed cones (Fig. 1), and the seeds support population growth among birds and small mammal species (*e.g.*, squirrels) with cascading trophic effects in subsequent seasons (Krebs et al., 2014; LaMontagne et al., 2013). The boom-and-bust cycle of mast seeding (Piovesan and Adams, 2001; Övergaard et al., 2007; LaMontagne and Boutin, 2009) can impart wide-ranging demographic effects on bird populations, enhancing reproduction and survival in mast years but then leading to reproductive failure and large-scale irruptive migration in the year after mast events occur (Koenig and Knops, 2001; Strong et al., 2015).

There is a growing recognition of the climatological teleconnections driving plant and animal populations across broad geographic scales (Zuckerberg et al., 2020). Regionally synchronized mast seeding patterns have been attributed to several evolutionary and climatological factors (Pearse et al., 2016). Evolutionarily, it has been proposed that

Fig. 1. Mature and open seed cones near the top of a white spruce in the Kluane region, Yukon, Canada. Photograph by Dr. Jalene LaMontagne (CC BY-NC).

phenological synchrony (Koenig et al., 2015) improves pollination efficiency (Moreira et al., 2014) and, at seed release, promotes predator satiation to enhance seed escape (Archibald et al., 2012; Janzen, 1971) to ensure local seedbed development and forest regeneration. White spruce (*Picea glauca* [Moench] Voss) and several other conifer genera are known as "two-year species" with seed cone development spanning two summers (three, for most *Pinus spp.*) from differentiation of reproductive buds through pollination, maturation of the resulting cones, and seed release in the subsequent autumn. Kelly et al. (2013) found that increasingly warmer summer temperatures over the two years prior to seed production constitute one of the most robust climatological signal associated with the magnitude of mast seeding, with net positive temperature differences between summers in the two years leading up to the mast event. Krebs et al. (2012) also suggested that a drier spring two years prior to reproduction is also related to larger cone crops. The summer temperature difference method has been used for successful prediction of mast years using climatological time series (Krebs et al., 2017; LaMontagne et al., 2020).

Efforts to document mast seeding patterns over time and space, and to identify exogenous factors promoting masting, have traditionally required intensive *in situ* surveys in multiple plant populations. As a result, it is challenging to capture the spatiotemporal characteristics of mast seeding at regional to sub-continental scales. White spruce is an ideal species for developing and testing new methods for masting detection, with most seed cones concentrated in the highly visible upper third of the tree crown in normal years and throughout the crown in mast years. Cone counts are obtained by observers in the field (LaMontagne et al., 2005) over multiple years to establish the long-term mean annual cone production to distinguish increased productivity in mast years (LaMontagne and Boutin, 2007, 2009).

Alternatively, satellite-based remote sensing provides an overhead view that covers broad geographic regions on quasi-regular cycles and over increasingly long time periods. The spatial and multispectral resolution of Landsat observations (~30 m pixels in six spectral bands) has proven useful for monitoring phenology (Jin and Eklundh, 2014), canopy structure (Matasci et al., 2018), primary productivity (Goetz and Prince, 1996), moisture status (Jin and Sader, 2005), disturbance effects (Jin and Sader, 2005; Masek et al., 2008), and post-disturbance recovery (Frazier et al., 2014; Hermosilla et al., 2016; Pickell et al., 2016) in relatively homogeneous evergreen boreal forests. Given that the full archive of Landsat images is now freely available for public use (Wulder et al., 2012, 2016), multispectral Landsat products provide numerous possibilities for methodological development to detect diverse changes in forest cover, productivity, phenology, disturbances, recovery, and overall health.

In this paper we test two alternative competing, but non-exclusive, approaches to detect mast-seeding patterns in white spruce forests using multispectral Landsat images: a photosynthesis-based approach, which we simplify as the "color hypothesis," and an approach based on observing canopy moisture content that we call the "moisture hypothesis." Our primary objective is to develop an empirical framework to distinguish between masting and non-mast years using only Landsat-based vegetation index (VI) observations. This work demonstrates the contribution of dense top-of-canopy seed crops to the Landsat signal during mast years, which points to potential uncertainties in discriminating among multiple drivers of inter-annual late-summer variability in evergreen conifer forests, which, in addition to masting, can include the effects of drought, climate variability and disturbance.

2. Study area

Our study locations include established Cooperative Ecological Monitoring Program (CEMP; www.zoology.ubc.ca/~krebs/kluane.html) sites located on Champagne and Aishihik First Nations (CAFN) Self-Governed Lands (Ogden and Innes, 2009) in southwestern Yukon, Canada (Fig. 2). The Kluane Boreal Forest Ecosystem Project (Krebs et al., 2001) and the ongoing CEMP study areas were established southeast of Kluane Lake and immediately northeast of the Kluane National Park and Reserve. Our sites are managed cooperatively for CAFN sustainable resource use and fire protection, especially following recent insect disturbances (Ogden and Innes, 2009; Paudel et al., 2015). The CEMP area is located in the Shakwak Trench (Zalatan and Gajewski, 2005), a quasi-linear topographic depression crossing southwestern Yukon that was formed by the Shakwak/Denali Fault Zone (Krebs and Boonstra, 2001) between the Kluane Range to the southwest and the Ruby Range to the northeast.

The study region lies on post-glacial loess soils (Krebs and Boonstra, 2001) dominated by interior boreal forest consisting primarily of white spruce and trembling aspen (*Populus tremuloides*) (Dale et al., 2001). The climate is cold continental (mean annual temperature −2.7 °C, σ = 1.4 °C during 1988–2017) with precipitation (mean annual total precipitation 273 mm liquid equivalent, σ = 63 mm during 1988–2017) predominantly during the growing season. Disturbances in the study region consist primarily of spruce beetle outbreaks, which caused surges in forest damage throughout the Kluane region in 1994–1998 (Dale et al., 2001; Garbutt et al., 2006) and in 2002–2005 (Garbutt et al., 2006; Pretzlaw et al., 2006; Hawkes et al., 2014). The last stand-replacing fire in the study area occurred in 1929 (Dale et al., 2001). The Kluane region has been the focus of numerous remote sensing studies focused on vegetation classification (*e.g.*, Franklin and Wulder, 2002) and detection of insect disturbances (Wulder et al., 2003; Berg et al., 2006).

2.1. Spruce cone surveys

The major evergreen conifer species in the Kluane area is white spruce (Dale et al., 2001). Observers conducted cone counts for a repeated set of 84–100 individual trees, separated by at least 30 m, at established grid locations within each site (Krebs et al., 2012, 2017). An observer in a stationary position on the ground, in a location where the top of the tree crown was visible, counted cones using a pair of binoculars. If the observer counted more than 100 visible cones on the tree *in situ*, the observer used a photograph of the tree to later tally the cones. The cone count was then converted to an estimate of cone production, the total number of cones on the tree, following LaMontagne et al. (2005). Based on cone production time series (Table 1; Fig. 3) we obtained the mean number of cones produced per tree over time for each site and then identified mast years using the standardized deviate method (LaMontagne and Boutin, 2007, 2009). We then expressed the masting state as a binary indicator (0 = non-mast year, 1 = mast year) for the Landsat analyses.
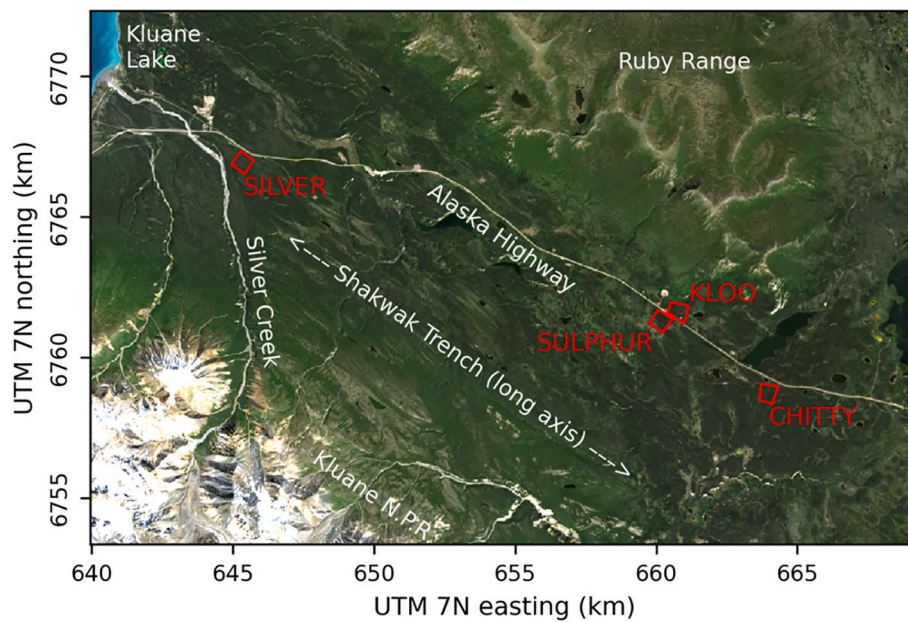
Fig. 2. Kluane region and selected study sites. Landsat 8 RGB (natural color) image (OLI bands 4, 3, 2) at WRS2 footprint P62R17 on 22 July 2014.

Table 1

Available CEMP cone count and Landsat time series details. Listed mast years are those marked in Fig. 3.

Site name	CEMP cone count dataset		Landsat pixels	Landsat scenes
	Time series	Mast years (as in Fig. 3)		
CHITTY	1991–2017	1998, 2010, 2014	369	192
KLOO	1988–2016	1993, 1998, 2005, 2010, 2014	203	200
SILVER	1999–2017	2005, 2010, 2014	369	197
SULPHUR	1988–2017	1993, 1998, 2005, 2010, 2014	215	200

Kluane-region cone production records collected for this work cover 30 years, from 1988 through 2017, and showed that mast years occurred at irregular, 4- to 7-year intervals: we identified five mast years (denoted "M") across our sites in M = 1993, 1998, 2005, 2010, and 2014 (Fig. 3). Not all of our selected sites demonstrated mast-level cone crops in all of the same years: the KLOO and SULPHUR sites (Fig. 2) in this study exhibited masting in all five mast years. However, the CHITTY site showed no such response in 1993 and 2005, with sitewide cone counts well below the long-term mean. The SILVER site, with a shorter time series (1999–2017), had mast years concurrent with those at the KLOO and SULPHUR sites within the available record. Overall, the dataset for statistical analysis included 105 site-years of information, including 16 masting site-years (Table 1, Fig. 3).

3. Methods

We describe here our primary competing but non-exclusive hypotheses for the detection of masting in spruce using Landsat VIs as well as how we approach time-series modeling and comparison with site-level observations. We do not address the magnitude of cone productivity, or site effects such as canopy density and closure, with these models.

3.1. Detection of masting via the color hypothesis

Our first test was derived from the visual observation of spruce cone senescence during late summer and as the cones open to release seeds in the autumn (Fig. 1). Cone production occurs within the top one-third of the crown of spruce trees in a normal year and covers much more of the tree crown in a mast year. Photosynthetic compounds in the developed cones (Aschan and Pfanz, 2003; Wang et al., 2006) either are resorbed or degrade during senescence. This browning at the tops of trees in a mast year across large swaths of spruce forest led us to hypothesize that mast years may appear similar to senescence in a Landsat image, though no such seasonal change would be expected at those locations in an evergreen forest. This loss of greenness in transition of the cones to non-photosynthetic vegetation is often measured with standard Landsat VIs based on the difference in the red and near-infrared (*NIR*) signals. Given that photosynthetic capacity is generally represented by the presence of green vegetation, we call this our "color hypothesis" for detection of masting.

We tested several photosynthesis-oriented VIs for which the band-based calculations are given in Table 2: the Normalized Difference Vegetation Index (NDVI: Sellers et al., 1996), which has low sensitivity to changes over time where vegetation density is high (Huete et al., 2002); the Enhanced Vegetation Index (EVI: Huete et al., 1997); and the greenness component of the Kauth–Thomas Tasseled Cap transformation (KTTC_GRN: Crist and Cicone, 1984; Crist, 1985; Crist and Kauth, 1986; Huang et al., 2002; Baig et al., 2014). We also examined a strictly color-based index known as the Green–Red Vegetation Index (GRVI: Motohka et al., 2010), which has been found useful for indicating the middle stages of autumn leaf coloration and senescence in deciduous forests (Muraoka et al., 2013). For all of these indexes, a loss of greenness and an increase in redness (together comprising the brown color) in the observation should lead to lower values in the autumn of a mast year, while the value of the index for an evergreen conifer forest canopy should remain relatively constant from summer through autumn in a non-mast year (barring other disturbances).

3.2. Detection of masting via the moisture hypothesis

Our second test arose from the observation that spruce (and many evergreen) seed cones are a concentrated repository of moisture in the tree canopy: during the last month of development, seed cone total moisture content can reach 60% (Cram and Worden, 1957), a level slightly greater than the typical summer moisture content of canopy spruce needles (~55%; Chrosciewicz, 1986). Once the seeds are fully
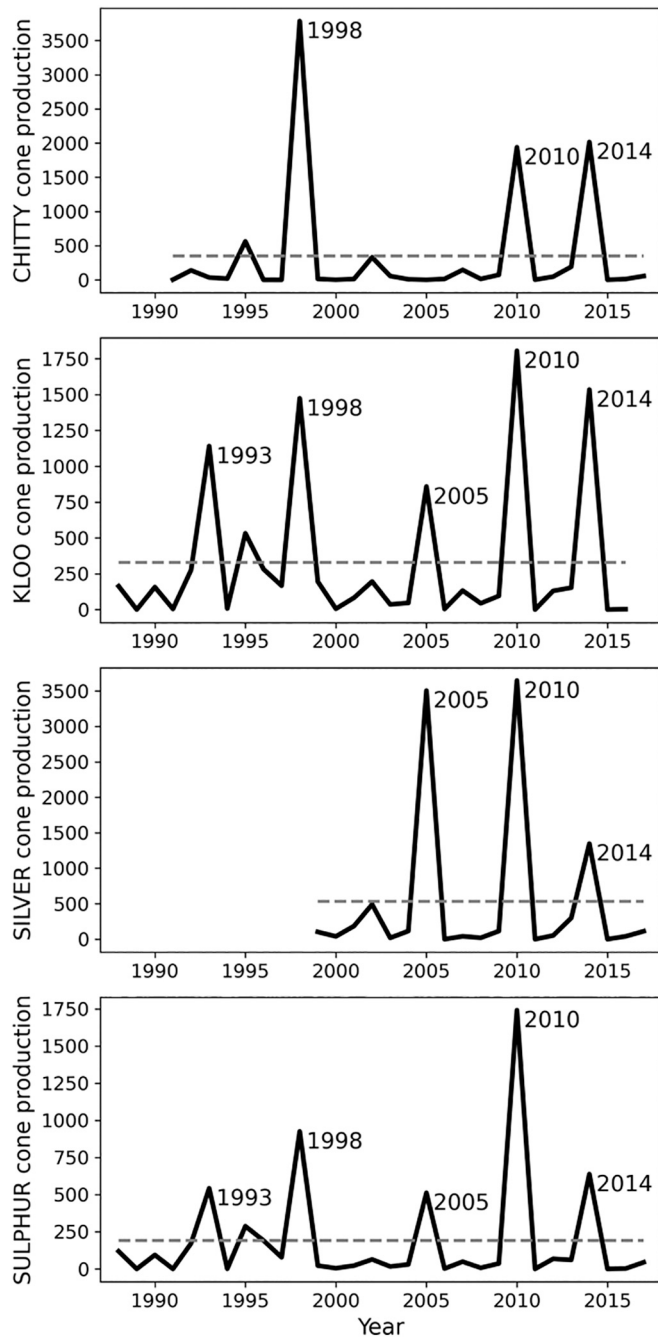
Fig. 3. Cone production time series at selected Kluane survey sites. The dashed line is the long-term mean for each site. Analyzed mast years are marked at the respective cone production peaks.

Table 2
Landsat multispectral vegetation index (VI) calculations.

Multispectral VI	Formula (Landsat TM/ETM+/OLI bands)	Primary Reference(s)
Green–Red Vegetation Index (*GRVI*)	$GRVI = \dfrac{Green - Red}{Green + Red}$	Motohka et al. (2010); Muraoka et al. (2013)
Normalized Difference Vegetation Index (*NDVI*)	$NDVI = \dfrac{NIR - Red}{NIR + Red}$	Sellers et al. (1996); Xie et al. (2008)
Enhanced Vegetation Index (*EVI*)	$EVI =$ $G \dfrac{NIR - Red}{NIR + C_1*Red - C_2*Blue + L}$ with $G = 2.5$, $C_1 = 6.0$, $C_2 = 7.5$, and $L = 1.0$	Huete et al. (1997)
Reduced Simple Ratio (*RSR*)	$RSR =$ $\left(\dfrac{NIR}{Red}\right)\left[1 - \dfrac{SWIR1 - SWIR1_{min}}{SWIR1_{max} - SWIR1_{min}}\right]$	Jordan (1969); Brown et al. (2000)
Normalized Difference Infrared Index (*NDII*) Moisture Index (*NDMI*) Water Index (*NDWI*)	$NDII = \dfrac{NIR - SWIR1}{NIR + SWIR1}$	Hardisky (1983); Gao (1996); Jin and Sader (2005)
Normalized Burn Ratio (*NBR*)	$NBR = \dfrac{NIR - SWIR2}{NIR + SWIR2}$	Key and Benson (2006); Miller and Thode (2007)
Kauth–Thomas Tasseled Cap (KTTC) transformation: Greenness (*KTTC_GRN*) and Wetness (*KTTC_WET*)	$KTTC\_GRN = -0.1603 * Blue - 0.2819 * Green - 0.4934 * Red + 0.7940 * NIR - 0.0002 * SWIR1 - 0.1446 * SWIR2$ $KTTC\_WET = 0.0315 * Blue + 0.2021 * Green + 0.3102 * Red + 0.1594 * NIR - 0.6806 * SWIR1 - 0.6109 * SWIR2$	Crist and Cicone (1984); Crist (1985); Crist and Kauth (1986); Huang et al. (2002); Baig et al. (2014)

effects on leaf area and canopy structure become visible (Isaacson et al., 2012), several *SWIR*-based indexes have demonstrated utility for early detection of numerous types of forest disturbances (Collins and Woodcock, 1996; Jin and Sader, 2005; Hais et al., 2009).

In remote sensing imagery, then, spruce cone opening and seed release can be viewed as a kind of forest disturbance, akin to drought response or a canopy defoliation event. In our analysis, we tested several VIs that use *SWIR* bands as indicators of vegetation moisture content: the Normalized Difference Infrared Index (NDII: Hardisky, 1983) that is also known as the Normalized Difference Moisture Index (NDMI: Jin and Sader, 2005) or the Normalized Difference Water Index (NDWI: Gao, 1996); the Normalized Burn Ratio (NBR: Key and Benson, 2006; Miller and Thode, 2007) that is commonly used for examinations of forest fire severity; and the wetness component of the Kauth–Thomas Tasseled Cap transformation (KTTC_WET: Crist and Cicone, 1984; Crist, 1985; Crist and Kauth, 1986). We also examine a hybrid index known as the Reduced Simple Ratio (RSR: Brown et al., 2000) based on the Simple Ratio (SR: Jordan, 1969), which we would classify on its own as a photosynthesis-based index, and the range of *SWIR1* values across the image to account for spatial variability in canopy moisture content. The RSR has been found useful for its relation to leaf area index (LAI) in some observations (Jordan, 1969; Brown et al., 2000; Chen et al., 2005).

3.3. Landsat image processing

We utilized Landsat scenes covering our study area for four overlapping footprints (WRS-2 designations P60R17, P60R18, P61R17, and P62R17) during July–September for all years in the cone count record, 1988–2017. In a mast year, this three-month period covers the end of the cone maturation period during summer and the time when cones open to release seeds in autumn. Observation of the senescence and drying of seed cones from late season imagery was limited by the progressively lower sun angle at the latitude of the Kluane region in the weeks leading

developed in late summer, the moisture supply to the cones is cut off and cones begin to senesce and dry to the point of seed release, which occurs at approximately 28% moisture content (Cram and Worden, 1957). This rapid drying of cone tissues over just a few weeks, to a moisture content about half that of the surrounding canopy, represents a significant loss of moisture that we hypothesize is detectable in multispectral Landsat images; we therefore call this our "moisture hypothesis" for the detection of masting. Landsat VIs that make use of the shortwave infrared (*SWIR1* and *SWIR2*) bands have been used to detect changes in forest canopy moisture content due to drought stress, defoliation, and fire (Hunt et al., 1987, 2011; White et al., 1996; Yilmaz et al., 2008; Townsend et al., 2012). Since many disturbance agents can affect transpiration function and canopy moisture content well before their

up to the autumnal equinox. Combined with mountainous terrain and the ~1030 LST Landsat overpass time, by the last week of September even the portions of the Kluane region outside of morning topographic shadows exhibited insufficient illumination for phenological analysis.

We downloaded 420 Landsat scenes for 1988–2017 from the USGS Landsat Collection 1 (C1; U.S. Geological Survey, 2018) *via* earthe xplorer.usgs.gov. Landsat C1 scenes have been geometrically and geographically registered and radiometrically calibrated (Level-1 products) and then converted to surface reflectance (Level-2 products) using *LEDAPS* (Masek et al., 2008, 2012) for Landsat 4/5 and 7 (TM/ETM+), and *LaSRC* (Vermote et al., 2018) for Landsat 8 (OLI). We used the supplied quality assurance data from *CFmask* (Zhu and Woodcock, 2012; Zhu et al., 2015; Foga et al., 2017) to mask clouds, cloud shadows, ice, and snow. To correct for topographic illumination, we used the geometric sun–canopy–sensor method (SCS; Gu and Gillespie, 1998), extended with the C-correction (Teillet et al., 1982; Meyer et al., 1993) applied to surface slope classes at 5° intervals (Vázquez-Jiménez et al., 2017). For these calculations we used the ASTER digital elevation model (DEM; Hirano et al., 2003) for the region. We calculated the eight VIs (Table 2) from the resulting corrected imagery.

Inspection of each site using Google Earth historical images and field reconnaissance (LaMontagne, pers. obs.) indicated that some portions of the KLOO and SULPHUR sites are not comprised of white spruce. Using Google Earth images, we digitized outlines of aspen stands and sparse canopy lowlands to exclude from analysis, leading to slightly different numbers of pixels per site (Table 1). We calculated the mean and standard deviation VI within the site for all dates in which at least 10% of the pixels were flagged as "good" and then removed duplicate pixels from the same path and date. The resulting data table contained 789 unique site observations across the eight VIs and four study sites (Fig. 4).

3.4. Weighted linear regressions for annual VI slopes

In conifer forests, both greenness and moisture related vegetation indexes decline from a summer peak into autumn, though not as dramatically as deciduous stands. Our approach was predicated on the expectation that in mast years, the slope of decline in a VI would be greater than a non-mast year due to the contribution from cones. We aimed to identify the effect of day-of-year on VI for all years with at least two image dates using the linear slope of the weighted least-squares (WLS) regression for the values of each VI values against the observation day-of-year (DOY) (Fig. 5). The regression weight of each data point w_i for each VI was devised to reduce the emphasis of scenes with fewer data points and greater variance:

$$w_{i,VI} = n_{px}/\sigma_{VI}^2 \tag{1}$$

where n_{px} is the number of pixels available within the site boundary, and σ_{VI} is the standard deviation of the VI values found in the site area for that scene. We then normalized these weights across all scenes available for that site. Accordingly, the scenes for each site with (1) the greatest pixel availability and (2) the lowest site-internal variance received the greatest weight in the WLS regression. Out of 105 possible site-years of data (matching the cone count dataset), we obtained WLS regression slopes for 101 site-years, with all 16 site-mast-years retained and only 4 non-masting site-years in the cone count dataset having just a single Landsat observation (1995 and 1997 at CHITTY, and 1997 at KLOO and SULPHUR).

We observed clear variability in the temporal patterns of the VIs, both between sites for any given year and over time within a single site, indicating variability in the timing of phenological stages. We standardized the annual regression slopes across years for each site and VI to normalize those differences in phenological stage and to facilitate including all site-years in a common statistical modeling approach. This enabled focusing the analysis on the differences between VI regression slopes during the mast and non-mast years to identify what fraction of the variability was related to the masting process, *e.g.*, the relationship between sites having $\mathcal{N}(0,1)$ and the regression slopes of season-ending VI decline. We note that the slope of VI with respect to DOY is also sensitive to solar illumination, but this effect is essentially normalized using our regression approach.
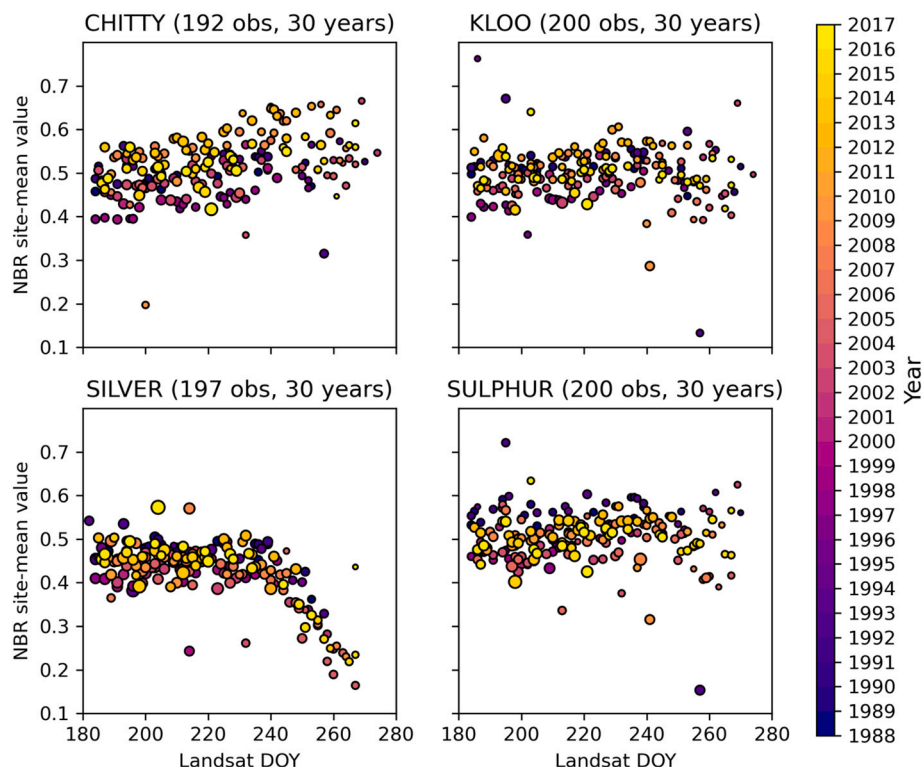

Fig. 4. Observations of site-mean NBR during 1988–2017, with marker size proportional to the observation weight as calculated using Eq. (1).
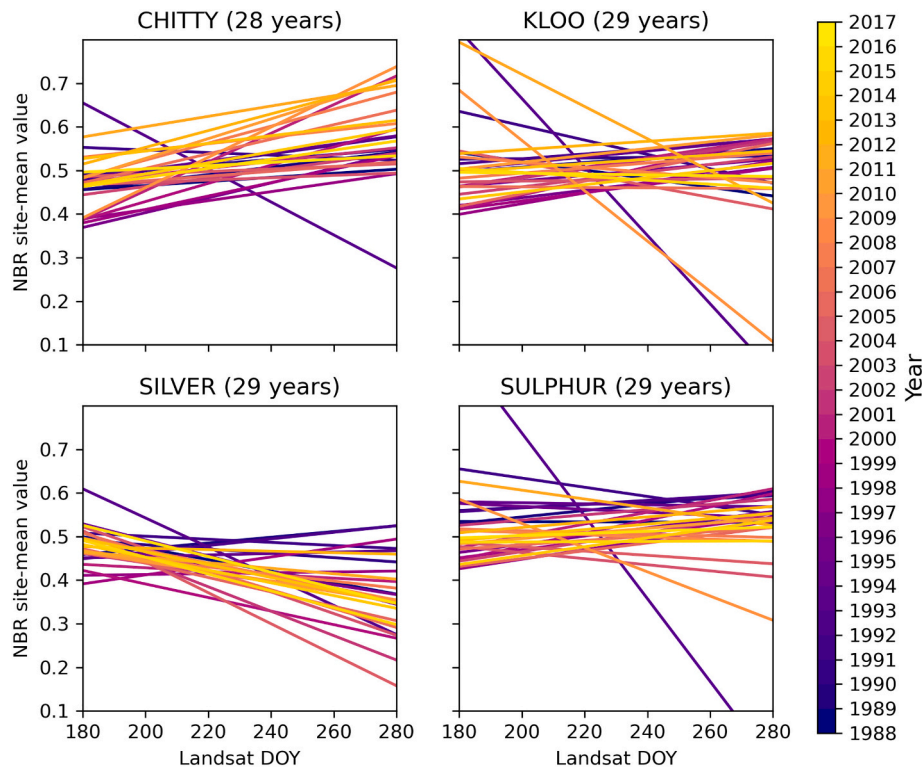
Fig. 5. Weighted least-squares (WLS) linear regressions of site-mean NBR (Fig. 4) on an annual basis during 1988–2017.

3.5. Generalized linear mixed-effects model (GLMM)

We used a generalized linear mixed-effects model (GLMM) with a binomial error distribution, known as a logistic model (Trexler and Travis, 1993), to predict masting in any particular year as a $\mathcal{N}(0, 1)$ function of the standardized annual VI slopes, with the general form:

$$P\left(mast\_year = 1 | \boldsymbol{X}_{VI,s,y}\right)$$
$$= \ell^{-1}\left[\beta_0 + \sum_{VI}\left(\beta_{VI}\,X_{VI,s,y}\right) + N\left(0, \sigma_s^2\right) + N\left(0, \sigma_y^2\right)\right] \quad (2)$$

using standardized time series $\boldsymbol{X}_{VI,s,y}$ for the VIs of interest in a given model, s and y representing site and year with their random effects included as the normal distributions, the intercept β_0 and the coefficients β_{VI} for each VI included in the model, and with the logit link function ℓ given as

$$\ell = ln\left[p/(1{-}p)\right] \quad (3)$$

with $p = \Pr(mast\_year = 1)$ the probability of a mast year. For comparison in our results, the corresponding null model has the form:

$$P\left(mast\_year = 1\right) = \ell^{-1}\left[\beta_0 + N\left(0, \sigma_s^2\right) + N\left(0, \sigma_y^2\right)\right] \quad (4)$$

where the VI components are excluded while the random factors (including regression intercept) are retained. We implemented this GLMM approach using the *Python* library *statsmodels* (Seabold and Perktold, 2010).

We used a model comparison approach using the Akaike Information Criterion (AIC) to select from a set of candidate models (Burnham and Anderson, 2002). Given relatively small sample sizes for each site in the dataset, we calculated the corrected *AIC* (*AICc*: Hurvich and Tsai, 1989; Cavanaugh, 1997) using the number of model parameters (including random factors) and the number of available observations. Models falling within $\Delta AICc \leq 2$ were considered functionally equivalent (Burnham and Anderson, 2002), even if other model-specific accuracy

metrics such as pseudo-R^2 differed. We performed model averaging of model predictions (Burnham and Anderson, 2002) for sets of models with $\Delta AICc \leq 2$. For each model, we report measures of model skill at prediction: pseudo-R^2 as an indicator of variance explained in the LMM, the confusion matrix, and Cohen's κ (Cohen, 1960) as an indicator of classification performance against chance. Due to the unbalanced distribution of our data between mast and non-mast years, we were especially interested in accounting for Type-II errors, in which accuracy is inflated by correctly classifying all non-mast years while incorrectly classifying mast years (see example in Supplemental Table 1). Models with $\kappa > 0$ are considered better than random, with some skill at prediction of observed masting in the site-year record. A value of $\kappa = 1$ would indicate perfect model-based prediction of the entire observation time series.

3.6. Software

Our full processing workflow, including input data and our *Python/Jupyter* statistical analysis notebooks, are available at https://github.com/megarcia/spruce_masting. Details on our processing workflow and necessary *Python* libraries are given in Appendix S1.

4. Results

4.1. Color-oriented VIs

None of our single-VI based logistic models to address the color hypothesis outperformed the null models in terms of *AICc* (Table 3), each with an accuracy of 84.2% but $\kappa = 0$ (*i.e.*, Type-II errors as illustrated in Table S1). Model coefficients for each VI bounded zero (Fig. 6a), but even so the direction of the coefficients tended positive, which is in contrast to our expectation of a negative slope (*i.e.*, steeper late season slopes of decrease in these color indexes during mast years).

Table 3

Results for single-VI logistic regression models using photosynthesis- and color-oriented VIs, ranked in order of increasing $\Delta AICc$. Note that correctly predicted non-mast years are not listed but are included in the calculation of overall accuracy and Cohen's κ. See Fig. 6a for individual logistic regression coefficients.

Logistic model VIs	pseudo-R^2	AICc	ΔAICc	Model weight	Correct mast years	Missed mast years	False alarms	Overall accuracy	Cohen's κ
null	0.011	93.4	——	——	0	16	0	0.842	0.000
KTTC_GRN	0.027	94.1	0.740	0.320	0	16	0	0.842	0.000
GRVI	0.027	94.2	0.801	0.311	0	16	0	0.842	0.000
EVI	0.017	95.0	1.626	0.206	0	16	0	0.842	0.000
NDVI	0.012	95.5	2.086	0.163	0	16	0	0.842	0.000
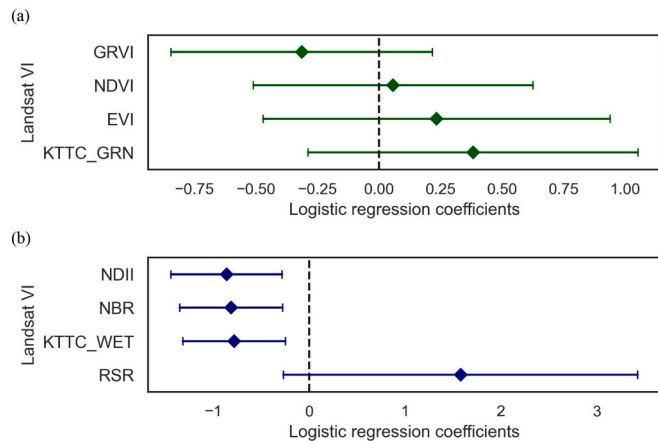
Fig. 6. GLMM regression coefficients and 95% confidence intervals for individual (a) color-oriented VIs and (b) moisture-oriented VIs. See Tables 3 and 4, respectively, for model accuracy metrics.

4.2. Moisture-oriented VIs

In contrast, logistic regressions using the moisture-oriented VIs NDII, NBR and Tasseled Cap Wetness exhibited an ability to identify mast years (Table 4), with statistically significant regression negative regression coefficients (Fig. 6b). The negative sign of the regression coefficients supports our hypothesis that mast years have a significantly steeper declining slope from summer to autumn in moisture-based VIs than non-mast years. Logistic regression using NDII produced the smallest *AICc* value and largest model *pseudo-R^2*. Models based on NBR and Tasseled Cap Wetness had $\Delta AICc \leq 2$ from that using NDII and were thus functionally equivalent to the NDII model, with all three of these VIs correctly predicting the same mast years and yielding the same $\kappa = 0.253$ value. The time series of standardized annual slopes for NDII, NBR, and KTTC_WET were highly correlated ($r > 0.7$; see Fig. S1) and it was thus not appropriate to combine them in a multi-VI regression (Dormann et al., 2013). Each model produced a single "false alarm" (type-I error) in addition to the large number of missed mast years (type-II errors). Our results for NDII, NBR and Tasseled Cap Wetness support the moisture hypothesis, although in a classification framework, each still misses a large fraction of the observed site-level mast-years in the cone-count record.

4.3. Two-VI logistic models

We tested whether combinations of one VI standardized slope from each category (color/greenness and moisture) would outperform single-VI models (Table 5, full results for all 16 possible combinations in Supplemental Table S2). Using two indexes, NDVI emerged as a useful support to the top two moisture-oriented single-VI logistic models (Table 5), NBR and NDII. Given that the site-year time series of NBR and NDII standardized annual regressions are correlated at $r = 0.95$ and are thus nearly interchangeable, and their two-VI logistic models have similar coefficients (compare Figs. 7 and S2), the resulting $\Delta AICc = 1.30$ suggests that these two models are functionally equivalent. Nevertheless, the NDVI + NBR model generates better results than the NDVI + NDII model in terms of prediction accuracy because of two fewer missed mast years and the lack of any false alarms (Table 5). As well, the NDVI + NBR model also outperforms the single models reported in Table 4 ($\kappa = 0.359$ *vs.* $\kappa = 0.253$). The coefficient for NDVI in the NDVI + NBR model was positive, and barely significant (Fig. 7), indicating the NDVI performs a balancing rather than additive role in the regression. The NDVI + NBR model accurately predicted two sites (KLOO and SULPHUR) in two mast years (1993 and 2010) and missed the other two sites in all years, including 2010 (Table 6).

4.4. Model averaging two-VI logistic models

Although the $\Delta AICc < 2$ between the NDVI + NBR and NDVI + NDII models, model averaging between the two candidate models yielded a result that was poorer than NDVI + NBR (Tables 5, 6, and S3), and only marginally better than the single moisture VI results (no false alarms compared to one; see Table 4).

4.5. Multi-VI logistic models

We also tested a combinatoric approach of an unrestricted number and combination of VIs in the logistic LMM framework. For the eight VIs listed in Table 2, and including the null model, we evaluated 256 possible logistic models, of which ten models were within $\Delta AICc \leq 2$ of the lowest *AICc* value (Table S4). The best model in terms of *AICc* used RSR + NBR (Table S4), and was equivalent to any of the moisture-oriented single-VI models, but was not quite as good as the best model produced by the categorically restricted two-VI logistic modeling approach (Table 5). The second-best model by the unrestricted approach used GRVI + RSR + NBR (with $\Delta AICc = 0.71$) but exhibited a better Cohen's κ (0.359 *vs.* 0.253), on account of one fewer missed mast year and one fewer false alarm. However, this model was no better than the

Table 4

Results for single-VI logistic regression models using moisture-oriented VIs, ranked in order of increasing $\Delta AICc$. Note that correctly predicted non-mast years are not listed but are included in the calculation of overall accuracy and Cohen's κ. See Fig. 6b for individual logistic regression coefficients.

Logistic model VIs	pseudo-R^2	AICc	ΔAICc	Model weight	Correct mast years	Missed mast years	False alarms	Overall accuracy	Cohen's κ
NDII	0.134	84.7	——	0.445	3	13	1	0.861	0.253
NBR	0.127	85.3	0.60	0.330	3	13	1	0.861	0.253
KTTC_WET	0.116	86.3	1.52	0.208	3	13	1	0.861	0.253
RSR	0.059	91.3	6.56	0.017	0	16	0	0.842	0.000
null	0.011	93.4	8.68	——	0	16	0	0.842	0.000

Table 5

Results for the top two-VI logistic regression models. Model weights incorporate only the two VI-based models listed here. Complete results for the restricted two-VI logistic regression models are given in Table S2. Note that correctly predicted non-mast years are not listed but are included in the calculation of overall accuracy and Cohen's κ. See Figs. 7 and S2 for individual logistic regression coefficients.

Logistic model VIs	pseudo-R^2	AICc	ΔAICc	Model weight	Correct mast years	Missed mast years	False alarms	Overall accuracy	Cohen's κ
NDVI + NBR	**0.188**	**82.1**	——	**0.657**	**4**	**12**	**0**	**0.881**	**0.359**
NDVI + NDII	0.173	83.4	1.30	0.343	2	14	1	0.851	0.169
null	0.011	93.4	11.31	——	0	16	0	0.842	0.000
average				**1.000**	**3**	**13**	**0**	**0.871**	**0.280**
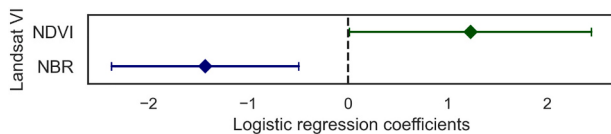
Fig. 7. LMM logistic regression coefficients and 95% confidence intervals for the best restricted two-VI model. See Tables 5 and S2 for model accuracy metrics and Table 6 for model prediction results.

Table 6

Prediction results for the best two-VI logistic regression using NDVI + NBR. Correctly predicted non-mast years (comprising 85 site-years) are not listed here. Model accuracy metrics are listed in Tables 5 and S2; logistic model coefficients for this result are shown in Fig. 7.

Site	Correctly predicted mast years (4)	Missed mast years (type-II error) (12)	False alarms (type-I error) (0)
CHITTY	——	1998, 2010, 2014	——
KLOO	1993, 2010	1998, 2005, 2014	——
SILVER	——	2005, 2010, 2014	——
SULPHUR	1993, 2010	1998, 2005, 2014	——

NDVI + NBR model (Table 6) and the model coefficient for the added variable GRVI was not significant (Fig. S4). Although multiple VIs from the same category often appeared together in successful models in the multi-VI approach, we consider these models to be ambiguous at best due to multicollinearity (Dormann et al., 2013) (see Fig. S1). As well, there was no benefit to model averaging using multiple VIs, nor did the prediction of sites improve over the two-VI models, although the years and sites that were predicted accurately did differ (compare Table 6 with Table S5).

5. Discussion

5.1. Overall findings

Under some conditions, mast seeding patterns in spruce can be detected using Landsat multispectral observations. We attribute this to the senescence and drying of seed cones during autumn in a mast year. We identified this trend as a function of the departure of the slope of decline in several moisture-oriented VIs from their summer baselines. This effect seems limited to moisture-oriented vegetation indexes such as NBR and NDII, while photosynthesis- and color-oriented (greenness) VIs demonstrate little potential on their own for detecting mast seeding patterns in conifer forests using multispectral satellite imagery. This outcome is a clear indication that, in remote sensing data, mast years in otherwise undisturbed coniferous forest areas exhibits a more robust response through changes in canopy moisture content than in color.

Multiple VIs in combination may improve our logistic modeling results: the combination of NDVI + NBR in a two-VI logistic model, and the combination of GRVI + RSR + NBR in a three-VI logistic model, were both more accurate than any single-VI model. While the detection of changes in canopy moisture might provide the bulk of the masting-related signal in the spruce forest, observations of photosynthetic

activity and/or color changes through the senescence process may provide an additional degree of discrimination. We note that the positive coefficients for the greenness VIs indicate that it balanced the influence of the moisture VIs. Specifically, NDVI may help discriminate sites with high slopes of decline in a moisture index due to some factor other than mast events. We have not examined the magnitude of cone productivity at each site-year or site effects such as canopy density and closure, which, if available, could help further refine models.

5.2. Disturbances and additional exogenous factors

As moisture-related VIs are often used to indicate various forest disturbances such as drought and some diseases (Collins and Woodcock, 1996; Jin and Sader, 2005; Masek et al., 2008), mast events might thus be treated as an occasional (quasi-regular) perturbation to the forest canopy that is detectable using standard methods of Landsat time series analysis (*e.g.*, Kennedy et al., 2010). Minimally, we demonstrate that mast events are apparent in the Landsat signal. We therefore recognize the strong possibility for confusion among analytical results for multiple disturbances that can have similar canopy responses. However, the disturbance-level signals may yet remain separable, as drought and disease are often creeping disturbances that show their effects over several years and through the full phenological cycle, unlike the isolated single-year effects of mast events on the conifer canopy that are apparent in our results (and that are apparent from late-season imagery). Analyses over a reasonable time period, spanning at least two mast events (approx. 5–10 years), might adequately distinguish mast years from some other disturbance agent in the study area.

However, the attack of spruce bark beetle in the Kluane region occurred in two major waves covering a similar period overall: beetle-induced forest damage was observed to surge in 1994–1998 (Dale et al., 2001; Garbutt et al., 2006) and in 2002–2005 (Garbutt et al., 2006; Pretzlaw et al., 2006; Hawkes et al., 2014), with ongoing lower-intensity damage before, after, and between. It is entirely likely that, with widespread beetle damage already present, any Landsat-based signal that we might have identified as masting activity in the observed 1998 and 2005 events (based on cone-count records) was obscured by the long-term background disturbance signal. This consideration of background disturbance conditions provides some explanation for the long gap between successful model-based mast-year detections at the KLOO and SULPHUR sites in 1993, before the onset of the beetle disturbance, and in 2010, after the initiation of forest recovery from the second surge in beetle activity.

These considerations do not, however, explain how the models missed the 2014 mast-year at all of our selected sites, as well as the failure of the models to detect any mast years at CHITTY, and the mixed results for model-based detection of masting at the SILVER site. For these, ongoing work must explore additional exogenous factors such as climatic (temperature and precipitation) influences on the physiological processes driving both mast seeding activity and canopy vigor, as well as on the variability of those influences among sites with different slopes, aspects, canopy closure, and so forth.

5.3. Site differences and non-random effects

It is well known that even nearby forest locations do not all behave consistently during mast events that are otherwise considered widespread in a region (LaMontagne and Boutin, 2007; LaMontagne et al., 2020). In the course of our analyses we noted significant variability among the selected sites in their observed masting record, followed by large variability in the predictions of our logistic LMM approach to mast-year discrimination. The CHITTY site, despite its white spruce composition and its proximity to the KLOO and SULPHUR sites (Fig. 2), differed from the other sites in both cone count time series (Fig. 3 and as shown in LaMontagne and Boutin, 2007) and VI-based modeling results. In particular, while the available time series indicated five mast events for the KLOO and SULPHUR sites, the CHITTY site clearly showed only three mast events over approximately the same period of record (Table 1; Fig. 3). One of those mast years, M = 2005, was indicated in cone-count time series at other sites but had no apparent observational signal at the CHITTY site, which we call a "missed mast event" in the regional context. At the same time, our best three-VI logistic LMM was able to detect mast events at the SILVER site in M = 2005 (Table S5), but unable to distinguish mast events at the KLOO and SULPHUR sites that year (possibly due to disturbance confusion, as mentioned above) and unable to detect mast events in subsequent years (M = 2010, 2014) at the SILVER site.

Comparisons of site-means and variability in annual cone-count productivity presented an interesting example of cross-site variability that we might take into account for mast/non-mast discrimination. The cone-count dataset (Fig. 3) indicated long-term mean productivity of μ = 328 cones/tree at the KLOO site, μ = 191 cones/tree at the SULPHUR site, and μ = 350 cones/tree at the SILVER site. In M = 2005, cone productivity during the mast events reached 858 cones/tree (~2.6 μ) at KLOO, 512 cones/tree (~2.7 μ) at SULPHUR, and 3505 cones/tree (~10 μ) at SILVER. The cone count at the SILVER site in 2002 (a non-mast year, according to the cone-count analysis) was 329 cones/tree, just less than the long-term mean cone count for that site, but equivalent to the long-term mean cone count at the KLOO site and much greater than the long-term mean at the SULPHUR site. In summary, a near-average year at a highly productive location (*e.g.*, SILVER) could resemble an above-average year at another less-productive location, leading to confusion regarding the significance of certain (*i.e.*, masting) years from the Landsat perspective. This suggests using absolute rather than relative cone counts, although that was not the basis for determining a mast year in LaMontagne and Boutin (2007, 2009), and that we might also require some level of normalization based on canopy cover or other site variables.

This points not just to the challenge of how to characterize a canopy process such as mast seeding for remote sensing analyses, but also to the broader challenge of integrating field data into remote sensing studies. We used a binary (mast/non-mast) classification, but our result would not be clear using the standardized deviate method of LaMontagne and Boutin (2009), which relies on relative cone counts for a single site over time instead of absolute productivity thresholds that might be translated between more- and less-productive sites. There is the potential here for a saturating effect based on both canopy and cone density: beyond a certain threshold in cone density that corresponds to a mast year at any number of nearby locations, and taking canopy density into account, highly productive sites in mast years may actually skew the regional cone count statistics. Normalizing cone-count density against canopy density could help with detection of a Landsat-based VI mast-year signal that stands out against background productivity and "normal" phenological variability in a non-mast year. However, if we cannot also normalize cone counts across study sites in some way that still allows indication of mast-year productivity, those data in high-productivity locations might need to be reserved from analysis as outliers.

5.4. Alternative approaches

Multiple site-specific and environmental factors affect the spatio-temporal variability of cone production over large areas. Detection algorithms based on remote sensing observations must remain robust to such spatiotemporal variability, and false negatives and false positives are in part attributable to this variability. Sites like CHITTY, with a slightly more open spruce canopy and mast seeding behavior that is clearly different from that at other nearby locations, suggest a need for more detailed study into possible site influences on mast seeding such as landscape position and aspect, soil types and moisture status, canopy closure, and micro-climatological patterns in temperature and precipitation. Implicit here is a gradual shift from our logistic LMM approach to a model framework with fewer random effects, toward greater consideration of explicit site effects and exogenous (*e.g.*, climatological) variables, and toward Gaussian or other statistical approaches to the distribution of cone-count observations instead of the binary mast/non-mast indication that was the simple focus of this work. Detection of mast events would certainly benefit from additional remote sensing derived datasets, such as canopy cover, but it must also be acknowledged that the derivation of such maps will also be confounded by the presence of mast events in some years.

Finally, tests of our approach in other evergreen conifer species, and eventually in mixed and hardwood stands where deciduous leaf senescence could cause signal confusion, are needed. Mast seeding processes, cone production volume, and cone placement within the tree crown differs considerably among species. In application, forest composition maps would then be required for the analyst to apply derived mast seeding classification rules according to species. Our methods may require adjustment in species where reproduction is consistently vertically distributed throughout the canopy, rather than concentrated near the top of the tree crown as in white spruce. From the overhead perspective, images with finer spatial resolution may enable better discrimination between masting and non-masting individuals and could aid in the calculation of canopy density as a potential, no-longer-random site factor in discrimination and/or productivity modeling of mast seeding activity based on remote sensing observations. However, our desire for more detailed observations must be weighed against the availability of indexes such as NDII and NBR, which require *SWIR* image bands that are not always available on high-spatial-resolution airborne and spaceborne platforms.

6. Conclusion

While the results from our logistical LMM approach indicate that moisture-oriented vegetation indexes perform more reliably than photosynthesis- and color-oriented Landsat-based VIs at discrimination between mast and non-mast site-years, the capacity for widespread accurate mapping of mast seeding using these methods is at present limited. Improvements in mapping would require additional inputs whose generation may also be sensitive to the presence of mast events. However, our results do demonstrate that mast seeding is a component of the signal in Landsat time series and could affect interpretations for other applications. Likewise, our results point to the need for care when interpreting VI time series for masting signals: the incorporation of ancillary information, including climatological records and field observations, will require significant additional work but might help distinguish between masting and other canopy-altering disturbances, such as insect disturbances and drought, that a less-informed time series analysis might confuse.

Our findings have the potential for widespread application, but with significant caveats. We provide a modeling framework that could guide future efforts to detect mast events and masting productivity in forests. Future work must address non-random site effects that can affect the outcome of simple mast/non-mast discrimination or the next step, addressing actual observations of cone production in mast and non-mast

years and their considerable variability across sites. Even if the detection of mast seeding events remains a challenge, analyses of the masting signal may also provide an explanation for phenological perturbations in VI time series where other causes, such as obvious disturbance agents, are not present. Nevertheless, the remote-sensing-based approach will be useful for the detection and measurement of mast seeding patterns across evergreen coniferous forest landscapes, especially in areas where ground-based observations and widespread cone-count data collection remain cost-prohibitive.

Author credit statement

Conceptualization and funding acquisition: BZ, JML, and PT. Methodology: MG, BZ, JML, and PT. Investigation and software: MG. Writing - original draft: MG, BZ, JML, and PT. Writing - review and editing: MG, BZ, JML, and PT.

Declaration of Competing Interest

The authors declare that they have no known competing financial interests or personal relationships that could have appeared to influence the work reported in this paper.

Acknowledgements

Appendix A. Supplementary data

Supplementary data to this article can be found online at https://doi.org/10.1016/j.rse.2020.112278.

References

Archibald, D.W., McAdam, A.G., Boutin, S., Fletcher, Q.E., Humphries, M.M., 2012. Within-season synchrony of a masting conifer enhances seed escape. The American Naturalist 179, 536–544. https://doi.org/10.1086/664623.

Aschan, G., Pfanz, H., 2003. Non-foliar photosynthesis – a strategy of additional carbon acquisition. Flora Morphol. Distrib. Funct. Ecol. Plants 198, 81–97. https://doi.org/10.1078/0367-2530-00080.

Baig, M.H.A., Zhang, L., Shuai, T., Tong, Q., 2014. Derivation of a tasselled cap transformation based on Landsat 8 at-satellite reflectance. Rem. Sens. Lett. 5, 423–431. https://doi.org/10.1080/2150704X.2014.915434.

Berg, E.E., David Henry, J., Fastie, C.L., De Volder, A.D., Matsuoka, S.M., 2006. Spruce beetle outbreaks on the Kenai peninsula, Alaska, and Kluane National Park and reserve, Yukon territory: relationship to summer temperatures and regional differences in disturbance regimes. For. Ecol. Manag. 227, 219–232. https://doi.org/10.1016/j.foreco.2006.02.038.

Brown, L., Chen, J.M., Leblanc, S.G., Cihlar, J., 2000. A shortwave infrared modification to the simple ratio for LAI retrieval in boreal forests: an image and model analysis. Remote Sens. Environ. 71, 16–25. https://doi.org/10.1016/S0034-4257(99)00035-8.

Burnham, K.P., Anderson, D.R., 2002. Model Selection and Inference: A Practical Information-Theoretic Approach, 2nd ed. Springer-Verlag, New York. https://doi.org/10.1007/b97636.

Cavanaugh, J.E., 1997. Unifying the derivations for the Akaike and corrected Akaike information criteria. Statist. Probab. Lett. 33, 201–208. https://doi.org/10.1016/S0167-7152(96)00128-9.

Chen, X., Vierling, L., Deering, D., Conley, A., 2005. Monitoring boreal forest leaf area index across a Siberian burn chronosequence: a MODIS validation study. Int. J. Remote Sens. 26, 5433–5451. https://doi.org/10.1080/01431160500285142.

Chrosciewicz, Z., 1986. Foliar moisture content variations in four coniferous tree species of Central Alberta. Can. J. For. Res. 16, 157–162. https://doi.org/10.1139/x86-029.

Cohen, J., 1960. A coefficient of agreement for nominal scales. Educ. Psychol. Meas. 20, 37–46. https://doi.org/10.1177/001316446002000104.

Collins, J.B., Woodcock, C.E., 1996. An assessment of several linear change detection techniques for mapping forest mortality using multitemporal Landsat TM data. Remote Sens. Environ. 56, 66–77. https://doi.org/10.1016/0034-4257(95)00233-2.

Cram, W.H., Worden, H.A., 1957. Maturity of white spruce cones and seed. For. Sci. 3, 263–269. https://doi.org/10.1093/forestscience/3.3.263.

Crist, E.P., 1985. A TM tasseled cap equivalent transformation for reflectance factor data. Remote Sens. Environ. 17, 301–306. https://doi.org/10.1016/0034-4257(85)90102-6.

Crist, E.P., Cicone, R.C., 1984. A physically-based transformation of thematic mapper data – the TM tasseled cap. IEEE Trans. Geosci. Remote Sens. 22, 256–263. https://doi.org/10.1109/tgrs.1984.350619.

Crist, E.P., Kauth, R.J., 1986. The tasseled cap de-mystified. Photogramm. Eng. Remote. Sens. 52, 81–86 (ISSN 0099-1112).

Dale, M.R.T., Francis, S., Krebs, C.J., Nams, V.O., 2001. Trees. In: Krebs, Charles, Boutin, S., Boonstra, R. (Eds.), Ecosystem Dynamics of the Boreal Forest: The Kluane Project. Oxford University Press, pp. 116–137.

Dormann, C.F., Elith, J., Bacher, S., Buchmann, C., Carl, G., Carré, G., García Marquéz, J. R., Gruber, B., Lafourcade, B., Leitão, P.J., Münkemüller, T., McClean, C., Osborne, P.E., Reineking, B., Schröder, B., Skidmore, A.K., Zurell, D., Lautenbach, S., 2013. Collinearity: a review of methods to deal with it and a simulation study evaluating their performance. Ecography 36, 27–46. https://doi.org/10.1111/j.1600-0587.2012.07348.x.

Foga, S., Scaramuzza, P.L., Guo, S., Zhu, Z., Dilley, R.D., Beckmann, T., Schmidt, G.L., Dwyer, J.L., Hughes, M.J., Laue, B., 2017. Cloud detection algorithm comparison and validation for operational Landsat data products. Remote Sens. Environ. 194, 379–390. https://doi.org/10.1016/j.rse.2017.03.026.

Franklin, S.E., Wulder, M.A., 2002. Remote sensing methods in medium spatial resolution satellite data land cover classification of large areas. Progr. Phys. Geogr. Earth Environ. 26, 173–205. https://doi.org/10.1191/0309133302pp332ra.

Frazier, R.J., Coops, N.C., Wulder, M.A., Kennedy, R., 2014. Characterization of aboveground biomass in an unmanaged boreal forest using Landsat temporal segmentation metrics. ISPRS J. Photogramm. Remote Sens. 92, 137–146. https://doi.org/10.1016/j.isprsjprs.2014.03.003.

Gao, B., 1996. NDWI—A normalized difference water index for remote sensing of vegetation liquid water from space. Remote Sens. Environ. 58, 257–266. https://doi.org/10.1016/S0034-4257(96)00067-3.

Garbutt, R., Hawkes, B., Allen, E., 2006. Spruce beetle and the forests of the Southwest Yukon. In: Natural Resources Canada, Canadian Forest Service. Pacific Forestry Centre, Victoria, BC. Information Report BC-X-406.

Goetz, S.J., Prince, S.D., 1996. Remote sensing of net primary production in boreal forest stands. Agric. For. Meteorol. 78, 149–179. https://doi.org/10.1016/0168-1923(95)02268-6.

Gu, D., Gillespie, A., 1998. Topographic normalization of Landsat TM images of forest based on subpixel sun–canopy–sensor geometry. Remote Sens. Environ. 64, 166–175. https://doi.org/10.1016/S0034-4257(97)00177-6.

Hais, M., Jonasova, M., Langhammer, J., Kucera, T., 2009. Comparison of two types of forest disturbance using multitemporal Landsat TM/ETM plus imagery and field vegetation data. Remote Sens. Environ. 113, 835–845. https://doi.org/10.1016/j.rse.2008.12.012.

Hardisky, M.A., Klemas, Smart, R.M., 1983. The influence of soil salinity, growth form, and leaf moisture on the spectral radiance of *Spartina alterniflora* canopies. Photogramm. Eng. Remote. Sens. 49, 77–83 (ISSN 0099-1112).

Hawkes, B., Alfaro, R., Waring, V., Berg, J., 2014. Response of southwest Yukon forests to spruce beetle: 2010 plot re-assessment. In: Natural Resources Canada, Canadian Forest Service. Pacific Forestry Centre, Victoria, BC. Information report BC-X-435.

Hermosilla, T., Wulder, M.A., White, J.C., Coops, N.C., Hobart, G.W., Campbell, L.B., 2016. Mass data processing of time series Landsat imagery: pixels to data products for forest monitoring. Int. J. Digit. Earth 9, 1035–1054. https://doi.org/10.1080/17538947.2016.1187673.

Hirano, A., Welch, R., Lang, H., 2003. Mapping from ASTER stereo image data: DEM validation and accuracy assessment. ISPRS J. Photogramm. Remote Sens. 57, 356–370. https://doi.org/10.1016/S0924-2716(02)00164-8.

Huang, C., Wylie, B., Yang, L., Homer, C., Zylstra, G., 2002. Derivation of a tasselled cap transformation based on Landsat 7 at-satellite reflectance. Int. J. Remote Sens. 23, 1741–1748. https://doi.org/10.1080/01431160110106113.

Huete, A.R., Liu, H.Q., Batchily, K., van Leeuwen, W.J., 1997. A comparison of vegetation indices over a global set of TM images for EOS-MODIS. Remote Sens. Environ. 59, 440–451. https://doi.org/10.1016/S0034-4257(96)00112-5.

Huete, A.R., Didan, K., Miura, T., Rodriguez, E.P., Gao, X., Ferreira, G., 2002. Overview of the radiometric and biophysical performance of the MODIS vegetation indices. Remote Sens. Environ. 83, 195–213. https://doi.org/10.1016/S0034-4257(02)00096-2.

Hunt, E.R., Rock, B.N., Nobel, P.S., 1987. Measurement of leaf relative water content by infrared reflectance. Remote Sens. Environ. 22, 429–435. https://doi.org/10.1016/0034-4257(87)90094-0.

Hunt, E.R., Li, L., Yilmaz, M.T., Jackson, T.J., 2011. Comparison of vegetation water contents derived from shortwave-infrared and passive-microwave sensors over Central Iowa. Remote Sens. Environ. 115, 2376–2383. https://doi.org/10.1016/j.rse.2011.04.037.

Hurvich, C.M., Tsai, C.-L., 1989. Regression and time series model selection in small samples. Biometrika 76, 297–307. https://doi.org/10.1093/biomet/76.2.297.

Isaacson, B.N., Serbin, S.P., Townsend, P.A., 2012. Detection of relative differences in phenology of forest species using Landsat and MODIS. Landsc. Ecol. 27, 529–543. https://doi.org/10.1007/s10980-012-9703-x.

Janzen, D.H., 1971. Seed predation by animals. Annu. Rev. Ecol. Syst. 2, 465–492. https://www.jstor.org/stable/2096937.

Jin, H., Eklundh, L., 2014. A physically based vegetation index for improved monitoring of plant phenology. Remote Sens. Environ. 152, 512–525. https://doi.org/10.1016/j.rse.2014.07.010.

Jin, S., Sader, S.A., 2005. Comparison of time series tasseled cap wetness and the normalized difference moisture index in detecting forest disturbances. Remote Sens. Environ. 94, 364–372. https://doi.org/10.1016/j.rse.2004.10.012.

Jordan, C.F., 1969. Derivation of leaf-area index from quality of light on the forest floor. Ecology 50, 663–666. https://doi.org/10.2307/1936256.

Kelly, D., 1994. The evolutionary ecology of mast seeding. Trends Ecol. Evol. 9, 465–470. https://doi.org/10.1016/0169-5347(94)90310-7.

Kelly, D., Geldenhuis, A., James, A., Holland, E.P., Plank, M.J., Brockie, R.E., Cowan, P.E., Harper, G.A., Lee, W.G., Maitland, M.J., Mark, A.F., Mills, J.A., Wilson, P.R., Byrom, A.E., 2013. Of mast and mean: differential-temperature cue makes mast seeding insensitive to climate change. Ecol. Lett. 16, 90–98. https://doi.org/10.1111/ele.12020.

Kennedy, R.E., Yang, Z., Cohen, W.B., 2010. Detecting trends in forest disturbance and recovery using yearly Landsat time series: 1. LandTrendr — Temporal segmentation algorithms. Remote Sens. Environ. 114, 2897–2910. https://doi.org/10.1016/j.rse.2010.07.008.

Key, C.H., Benson, N.C., 2006. Landscape Assessment (LA): Sampling and Analysis Methods. USDA Forest Service, Rocky Mountain Research Station, General Technical Report RMRS-GTR-164-CD, p. 55.

Koenig, W.D., Knops, J.M.H., 1998. Scale of mast-seeding and tree-ring growth. Nature 396, 225–226. https://doi.org/10.1038/24293.

Koenig, W.D., Knops, J.M.H., 2001. Seed-crop size and eruptions of north American boreal seed-eating birds. J. Anim. Ecol. 70, 609–620. https://doi.org/10.1046/j.1365-2656.2001.00516.x.

Koenig, W.D., Knops, J.M.H., Carmen, W.J., Pearse, I.S., 2015. What drives masting? The phenological synchrony hypothesis. Ecology 96, 184–192. https://doi.org/10.1890/14-0819.1.

Krebs, C., Boonstra, R., 2001. The Kluane Region. In: Krebs, Charles, Boutin, S., Boonstra, R. (Eds.), Ecosystem Dynamics of the Boreal Forest: The Kluane Project. Oxford University Press, pp. 9–24.

Krebs, C.J., Boutin, S., Boonstra, R., 2001. Ecosystem Dynamics of the Boreal Forest. Oxford University Press, New York, p. 544. + illus., ISBN 9780195133936.

Krebs, C.J., LaMontagne, J.M., Kenney, A.J., Boutin, S., 2012. Climatic determinants of white spruce cone crops in the boreal forest of southwestern Yukon. Botany 90, 113–119. https://doi.org/10.1139/b11-088.

Krebs, C.J., Boonstra, R., Boutin, S., Sinclair, A.R.E., Smith, J.N.M., Gilbert, B.S., Martin, K., O'Donoghue, M., Turkington, R., 2014. Trophic dynamics of the boreal forests of the Kluane region. Arctic 67 (Suppl. 1), 71–81. https://doi.org/10.14430/arctic4350.

Krebs, C.J., O'Donoghue, M., Taylor, S., Kenney, A.J., Hofer, E.J., Boutin, S., 2017. Predicting white spruce cone crops in the boreal forests of southern and Central Yukon. Can. J. For. Res. 47, 47–52. https://doi.org/10.1139/cjfr-2016-0180.

LaMontagne, J.M., Boutin, S., 2007. Local-scale synchrony and variability in mast seed production patterns of *Picea glauca*. J. Ecol. 95, 991–1000. https://doi.org/10.1111/j.1365-2745.2007.01266.x.

LaMontagne, J.M., Boutin, S., 2009. Quantitative methods for defining mast-seeding years across species and studies. J. Veg. Sci. 20, 745–753. https://doi.org/10.1111/j.1654-1103.2009.01068.x.

LaMontagne, J.M., Peters, S., Boutin, S., 2005. A visual index for estimating cone production for individual white spruce trees. Can. J. For. Res. 35, 3020–3026. https://doi.org/10.1139/x05-210.

LaMontagne, J.M., Williams, C.T., Donald, J.L., Humphries, M.M., McAdam, A.G., Boutin, S., 2013. Linking intraspecific variation in territory size, cone supply, and survival of north American red squirrels. J. Mammal. 94, 1048–1058. https://doi.org/10.1644/12-MAMM-A-245.1.

LaMontagne, J.M., Pearse, I.S., Greene, D.F., Koenig, W.D., 2020. Mast seeding patterns are asynchronous at a continental scale. Nature Plants 6, 460–465. https://doi.org/10.1038/s41477-020-0647-x.

Masek, J.G., Huang, C., Wolfe, R., Cohen, W., Hall, F., Kutler, J., Nelson, P., 2008. North American forest disturbance mapped from a decadal Landsat record. Remote Sens. Environ. 112, 2914–2926. https://doi.org/10.1016/j.rse.2008.02.010.

Masek, J.G., Vermote, E.F., Saleous, N., Wolfe, R., Hall, F.G., Huemmrich, F., Gao, F., Kutler, J., Lim, T.K., 2012. LEDAPS Landsat Calibration, Reflectance, Atmospheric Correction Preprocessing Code. Model product, available on-line from. Oak Ridge National Laboratory Distributed Active Archive Center, Oak Ridge, Tennessee, USA. https://doi.org/10.3334/ORNLDAAC/1080.

Matasci, G., Hermosilla, T., Wulder, M.A., White, J.C., Coops, N.C., Hobart, G.W., Zald, H.S.J., 2018. Large-area mapping of Canadian boreal forest cover, height,

biomass and other structural attributes using Landsat composites and lidar plots. Remote Sens. Environ. 209, 90–106. https://doi.org/10.1016/j.rse.2017.12.020.

Meyer, P., Itten, K.I., Kellenberger, T., Sandmeier, S., Sandmeier, R., 1993. Radiometric corrections of topographically induced effects on Landsat TM data in an alpine environment. ISPRS J. Photogramm. Remote Sens. 48, 17–28. https://doi.org/10.1016/0924-2716(93)90028-L.

Miller, J.D., Thode, A.E., 2007. Quantifying burn severity in a heterogeneous landscape with a relative version of the delta normalized Rurn ratio (dNBR). Remote Sens. Environ. 109, 66–80. https://doi.org/10.1016/j.rse.2006.12.006.

Moreira, X., Abdala-Roberts, L., Linhart, Y.B., Mooney, K.A., 2014. Masting promotes individual- and population-level reproduction by increasing pollination efficiency. Ecology 95, 801–807. https://doi.org/10.1890/13-1720.1.

Motohka, T., Nasahara, K.N., Oguma, H., Tsuchida, S., 2010. Applicability of green-red vegetation index for remote sensing of vegetation phenology. Remote Sens. 2, 2369–2387. https://doi.org/10.3390/rs2102369.

Muraoka, H., Noda, H.M., Nagai, S., Motohka, T., Saitoh, T.M., Nasahara, K.N., Saigusa, N., 2013. Spectral vegetation indices as the indicator of canopy photosynthetic productivity in a deciduous broadleaf forest. J. Plant Ecol. 6, 393–407. https://doi.org/10.1093/jpe/rts037.

Ogden, A., Innes, J., 2009. Application of structured decision making to an assessment of climate change vulnerabilities and adaptation options for sustainable forest management. Ecol. Soc. 14. https://doi.org/10.5751/ES-02771-140111.

Övergaard, R., Gemmel, P., Karlsson, M., 2007. Effects of weather conditions on mast year frequency in beech (*Fagus sylvatica* L.) in Sweden. Forestry 80, 555–565. https://doi.org/10.1093/forestry/cpm020.

Paudel, S.K., Nitschke, C.R., Simard, S.W., Innes, J.L., 2015. Regeneration dynamics of white spruce, trembling aspen, and balsam poplar in response to disturbance, climatic, and edaphic factors in the cold, dry boreal forests of the Southwest Yukon, Canada. J. For. 113, 463–474. https://doi.org/10.5849/jof.14-086.

Pearse, I.S., Koenig, W.D., Kelly, D., 2016. Mechanisms of mast seeding: resources, weather, cues, and selection. New Phytol. 212, 546–562. https://doi.org/10.1111/nph.14114.

Pickell, P.D., Hermosilla, T., Frazier, R.J., Coops, N.C., Wulder, M.A., 2016. Forest recovery trends derived from Landsat time series for North American boreal forests. Int. J. Remote Sens. 37, 138–149. https://doi.org/10.1080/2150704X.2015.1126375.

Piovesan, G., Adams, J.M., 2001. Masting behaviour in beech: linking reproduction and climatic variation. Can. J. Bot. 79, 1039–1047. https://doi.org/10.1139/b01-089.

Pretzlaw, T., Trudeau, C., Humphries, M.M., LaMontagne, J.M., Boutin, S., 2006. Red squirrels (*Tamiasciurus hudsonicus*) feeding on spruce bark beetle (*Dendroctonus rufipennis*): energetic and ecological implications. J. Mammal. 87, 909–914. https://doi.org/10.1644/05-MAMM-A-310R1.1.

Seabold, S., Perktold, J., 2010. Statsmodels: econometric and statistical modeling with Python. In: Proceedings of the 9th Python in Science Conference, Austin, Texas, 92–96. https://doi.org/10.25080/Majora-92bf1922.

Sellers, P.J., Tucker, C.J., Collatz, G.J., Los, S.O., Justice, C.O., Dazlich, D.A., Randall, D.A., 1996. A revised land surface parameterization (SiB2) for atmospheric GCMs. Part II: The generation of global fields of terrestrial biophysical parameters from satellite data. J. Clim. 9, 706–737. https://doi.org/10.1175/1520-0442(1996)009<0706:ARLSPF>2.0.CO;2.

Strong, C., Zuckerberg, B., Betancourt, J.L., Koenig, W.D., 2015. Climatic dipoles drive two principal modes of north American boreal bird irruption. Proc. Natl. Acad. Sci. 112, E2795–E2802. https://doi.org/10.1073/pnas.1418414112.

Teillet, P.M., Guindon, B., Goodenough, D.G., 1982. On the slope-aspect correction of multispectral scanner data. Can. J. Remote. Sens. 8, 84–106. https://doi.org/10.1080/07038992.1982.10855028.

Townsend, P.A., Singh, A., Foster, J.R., Rehberg, N.J., Kingdon, C.C., Eshleman, K.N., Seagle, S.W., 2012. A general Landsat model to predict canopy defoliation in broadleaf deciduous forests. Remote Sens. Environ. 119, 255–265. https://doi.org/10.1016/j.rse.2011.12.023.

Trexler, J.C., Travis, J., 1993. Nontraditional regression analyses. Ecology 74, 1629–1637. https://doi.org/10.2307/1939921.

U.S. Geological Survey, 2018. Landsat collections. In: Report 2018-3049 (Fact Sheet). USGS Publications Warehouse, Reston, Virginia, USA, p. 2. https://doi.org/10.3133/fs20183049.

Vázquez-Jiménez, R., Romero-Calcerrada, R., Ramos-Bernal, R.N., Arrogante-Funes, P., Novillo, C.J., 2017. Topographic correction to Landsat imagery through slope classification by applying the SCS + C method in mountainous forest areas. ISPRS Int. J. Geo Inf. 6, 287. https://doi.org/10.3390/ijgi6090287.

Vermote, E., Roger, J.C., Franch, B., Skakun, S., 2018. LaSRC (Land Surface Reflectance Code): Overview, application and validation using MODIS, VIIRS, LANDSAT and Sentinel 2 data. IGARSS 2018–2018. IEEE International Geoscience and Remote Sensing Symposium, Valencia, Italy. https://doi.org/10.1109/IGARSS.2018.8517622.

Wang, W.-J., Watanabe, Y., Endo, I., Kitaoka, S., Koike, T., 2006. Seasonal changes in the photosynthetic capacity of cones on a larch (*Larix kaempferi*) canopy. Photosynthetica 44, 345–348. https://doi.org/10.1007/s11099-006-0034-5.

White, J.D., Ryan, K.C., Key, C.C., Running, S.W., 1996. Remote sensing of forest fire severity and vegetation recovery. Int. J. Wildland Fire 6, 125–136. https://doi.org/10.1071/wf9960125.

Wulder, M.A., Dechka, J.A., Gillis, M.A., Luther, J.E., Hall, R.J., Beaudoin, A., Franklin, S.E., 2003. Operational mapping of the land cover of the forested area of Canada with Landsat data: EOSD land cover program. For. Chron. 79, 1075–1083. https://doi.org/10.5558/tfc791075-6.

Wulder, M.A., Masek, J.G., Cohen, W.B., Loveland, T.R., Woodcock, C.E., 2012. Opening the archive: how free data has enabled the science and monitoring promise of

Landsat. Remote Sens. Environ. 122, 2–10. https://doi.org/10.1016/j.rse.2012.01.010.

Wulder, M.A., White, J.C., Loveland, T.R., Woodcock, C.E., Belward, A.S., Cohen, W.B., Fosnight, E.A., Shaw, J., Masek, J.G., Roy, D.P., 2016. The global Landsat archive: status, consolidation, and direction. Remote Sens. Environ. 185, 271–283. https://doi.org/10.1016/j.rse.2015.11.032.

Xie, Y., Sha, Z., Yu, M., 2008. Remote sensing imagery in vegetation mapping: a review. J. Plant Ecol. 1, 9–23. https://doi.org/10.1093/jpe/rtm005.

Yilmaz, M.T., Hunt, E.R., Jackson, T.J., 2008. Remote sensing of vegetation water content from equivalent water thickness using satellite imagery. Remote Sens. Environ. 112, 2514–2522. https://doi.org/10.1016/j.rse.2007.11.014.

Zalatan, R., Gajewski, K., 2005. Tree-ring analysis of five *Picea glauca*-dominated sites from the interior boreal forest in the Shakwak trench, Yukon territory, Canada. Polar Geogr. 29, 1–16. https://doi.org/10.1080/789610162.

Zhu, Z., Woodcock, C.E., 2012. Object-based cloud and cloud shadow detection in Landsat imagery. Remote Sens. Environ. 118, 83–94. https://doi.org/10.1016/j.rse.2011.10.028.

Zhu, Z., Wang, S., Woodcock, C.E., 2015. Improvement and expansion of the Fmask algorithm: cloud, cloud shadow, and snow detection for Landsats 4–7, 8, and sentinel 2 images. Remote Sens. Environ. 159, 269–277. https://doi.org/10.1016/j.rse.2014.12.014.

Zuckerberg, B., Strong, C., LaMontagne, J.M., St. George, S., Betancourt, J.L., Koenig, W.D., 2020. Climate dipoles as continental drivers of plant and animal populations. Trends Ecol. Evol. 35, 440–453. https://doi.org/10.1016/j.tree.2020.01.010.